Intertwined Rashba, Dirac, and Weyl Fermions in Hexagonal Hyperferroelectrics

Domenico Di Sante,[1,2,*] Paolo Barone,[2,5] Alessandro Stroppa,[2] Kevin F. Garrity,[3] David Vanderbilt,[4] and Silvia Picozzi[2]
[1]*Institut für Theoretische Physik und Astrophysik, Universität Würzburg, Am Hubland Campus Süd, Würzburg 97074, Germany*
[2]*Consiglio Nazionale delle Ricerche (CNR-SPIN), Via Vetoio, L'Aquila 67100, Italy*
[3]*Material Measurement Laboratory, National Institute of Standards and Technology, Gaithersburg Maryland, 20899, USA*
[4]*Department of Physics and Astronomy, Rutgers University, Piscataway, New Jersey 08854, USA*
[5]*Graphene Labs, Istituto Italiano di Tecnologia, via Morego 30, 16163 Genova, Italy*
(Received 14 January 2016; published 8 August 2016)

By means of density functional theory based calculations, we study the role of spin-orbit coupling in the new family of *ABC* hyperferroelectrics [Garrity, Rabe, and Vanderbilt Phys. Rev. Lett. **112**, 127601 (2014)]. We unveil an extremely rich physics strongly linked to ferroelectric properties, ranging from the electric control of bulk Rashba effect to the existence of a three-dimensional topological insulator phase, with concomitant topological surface states even in the ultrathin film limit. Moreover, we predict that the topological transition, as induced by alloying, is followed by a Weyl semimetal phase of finite concentration extension, which is robust against disorder, putting forward hyperferroelectrics as promising candidates for spin-orbitronic applications.

DOI: 10.1103/PhysRevLett.117.076401

Introduction.—Spin-orbit coupling (SOC) is a relativistic interaction that gives rise to a rich variety of interesting phenomena in solid state physics, ranging from topological quantum phases of matter to Rashba- or Dresselhaus-like spin splitting effects. In the former case, fully spin-polarized massless Dirac fermions appear at the surface of topological insulators (TIs), showing protected metallic surface states despite their bulk insulating character [1,2]. In the latter case, which is realized at surfaces or interfaces as due to a structural inversion asymmetry of the confinment potential or in noncentrosymmetric materials, spin-splitting effects on the bands of massive fermions appear, which may ultimately give rise to a spin-Hall effect. [3,4] The presence of strong spin-momentum locking in both systems allows, in principle, for an all-electric control of the electron spins, putting forward these material systems as ideal candidates for new spintronic applications.

Interestingly, SnTe, the first proposed topological crystalline insulator (TCI) in its centrosymmetric structure [5], was predicted to host a coexistence of Rashba and topological properties when the inversion symmetry is broken at low temperature by a ferroelectric instability. [6] In fact, the breaking of inversion symmetry alone is not expected to suppress the topological insulating phase, as long as the relevant symmetries responsible of the topological protection are maintained. On the other hand, the gapless Dirac states at the surface of an acentric TI are expected to have completely different shapes on inequivalent sides of the material; as a consequence, electrons would be separated into nonequivalent halves on opposite surfaces (showing, e.g., charge carriers of different p/n types or parallel spin-polarization pattern), possibly leading to new features and spintronic functionalities [7–10]. Recently it has been shown that the phase transition from a noncentrosymmetric three-dimensional topological insulator to a normal insulator always hosts an intermediate Weyl semimetal phase [11–14]. The interplay of the above features with ferroelectricity has not been considered so far, despite the fact that ferroelectrics, i.e., polar materials with switchable electric polarization, could provide an additional degree of freedom for controlling and/or manipulating the electronic properties of relativistic fermions. A very large Rashba spin-splitting in the bulk electronic structure has been reported for tellurohalides, a family of noncentrosymmetric, but not ferroelectric, semiconductors with strong SOC [15–18]. After that, it has been shown that ferroelectric polarization may allow the permanent control of bulk Rashba-like effects, such as the switching of spin texture upon reversal of ferroelectric polarization, thus allowing for new nonvolatile functionalities in spintronic devices. GeTe, one of the oldest ferroelectrics, has been considered as the prototypical ferroelectric Rashba semiconductor (FERSC) [19–21].

Most of the well-known conventional ferroelectrics belong to the class of insulating transition-metal perovskite oxides. In these systems, the ferroelectric transition arises typically from an unstable zone-centered transverse optic (TO) mode associated with a symmetry-lowering polar distortion of the bulk material [22]. However, a thin film of such (proper) ferroelectric materials will experience large depolarization fields arising from surface charge accumulations, which would produce a strong electric field counteracting the polar displacemen+ts. It has been shown that the depolarization field completely suppresses the ferroelectric distortion in films thinner than ∼10 nm [23]. This issue, together with their strong insulating character, make conventional proper ferroelectrics unsuitable for real technological applications aiming at integrating ferroelectricity and relativistic effects in low-dimensional devices. However,

very recently, a new class of ferroelectric materials, called "hyperferroelectrics," has been proposed [24]. The interesting property of these systems is their ability to spontaneously polarize even in the presence of an unscreened depolarization field. This feature arises from an additional instability of a longitudinal optic (LO) mode besides the usual TO mode instability characteristic of proper ferroelectrics [24]. Garrity and co-workers proposed that hexagonal *ABC* ferroelectric semiconductors with LiGaGe structure are suitable candidates for hyperferroelectricity [25,26].

In this study, we focus on the relativistic properties of these materials by means of accurate density functional theory (DFT) calculations. [26] We show that hexagonal hyperferroelectrics (HHs) belong to and broaden the class of FERSC materials, where the bulk Rashba spin texture can be fully controllable by the ferroelectric polarization. Since hyperferroelectrics are less sensitive to surface effects, the switchable bulk Rashba features are expected to survive in low-dimensional systems, which is clearly an appealing property for spintronic applications. Furthermore, we show that HHs can host a topologically nontrivial $\mathcal{Z}_2$ quantum phase with symmetry-protected *inequivalent and tunable* surface states coexisting with Rashba-like features. While the topological phase is predicted to survive up to ultrathin films, we also show that a phase transition from topological insulator to a Weyl semimetal and eventually to a normal insulator can be realized by chemical doping and alloying.

Results and discussions.—We begin our analysis by calculating the relativistic bulk band structure of the hyperferroelectric NaZnSb. In Fig. 1(a), a direct gap is clearly visible at the Γ point, where the Sb orbital character dominates the valence low-energy states, while an equally mixed Sb and Zn character is found in the conduction bands. The expected dispersion of a Kramers doublet around the Γ point can be generally deduced from the knowledge of the symmetry properties of the corresponding group of k. Since all considered hexagonal *ABC* ferroelectric semiconductors belong to space group $P6_3mc$ (no. 186), the little group of Γ is C_{6v}, consisting of twofold C_2, threefold C_3, and sixfold C_6 rotations along the z direction and of three mirror operations M_v about a vertical reflection plane (containing the ΓM line) and three M_d about a dihedral reflection plane (containing the ΓK line). For spin 1/2 electrons, C_n rotations can be represented as $e^{-i\sigma_z\pi/n}$, and the two mirror operations as $M_v = i\sigma_x$ and $M_d = i\sigma_y$, where $\sigma_{x,y,z}$ are the Pauli matrices for spin degrees of freedom. Imposing the invariance of the $\boldsymbol{k}\cdot\boldsymbol{p}$ Hamiltonian around Γ with respect to the crystalline symmetry and time-reversal symmetry $T = i\sigma_y\mathcal{K}$ (where $\mathcal{K}$ is complex conjugation), one finds $H_\Gamma = (k_x^2 + k_y^2)/2m_{xy}^* + k_z^2/2m_z^* + \alpha_R(k_x\sigma_y - k_y\sigma_x)$, where the last term describes a Rashba coupling, while m_{xy}^*, m_z^* are the in-plane and out-of-plane effective masses. Third-order terms leading to warping of the bands are symmetry forbidden, since they would break the invariance with respect to C_2 and C_6 rotations. A zoom around the Γ point highlights typical Rashba-like spin-split bands, both in the valence and conduction regions, as shown in Fig. 1(b) along the two orthogonal k_x (ΓK) and k_y (ΓM) axes.

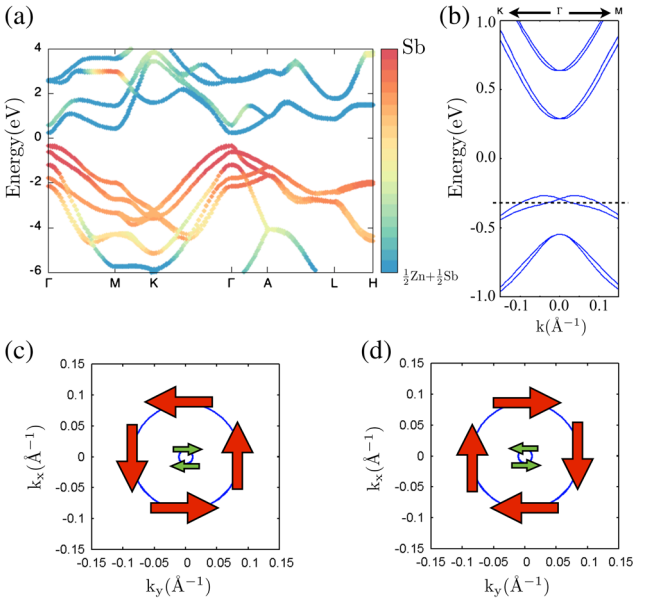

FIG. 1. (a) Relativistic bandstructure of NaZnSb along the high-symmetry lines of the hexagonal Brillouin zone [26]. Colors highlight the atomic orbital character, from Sb orbitals (red) to an equal mix of Zn and Sb orbitals (blue). (b) Zoom at the Γ point around the Fermi level along the Γ K and Γ M directions. A Rashba type spin-splitting occurs at the valence, as well as conduction, bands. (c) Spin texture of the valence bands at −0.30 eV [dashed line in (b)], with spins circularly rotating on both branches. (d) Spin-texture reversing after the switching of the bulk polarization.

An energy cut below the degeneracy point at Γ reveals an isotropic Fermi surface in the k_xk_y plane, with two concentric circular branches [see Fig. 1(c)]. Spins, always tangential to the isoenergy curves and perpendicular to momenta, rotate in opposite ways in the two branches, consistently with the $\boldsymbol{k}\cdot\boldsymbol{p}$ model sketched above. We can estimate the strength of the Rashba effect through the energy and momentum offsets E_R and k_R locating the band extrema via the Rashba parameter $\alpha_R = 2E_R/k_R$. For NaZnSb we find $k_R \approx 0.038$ Å^{-1}, $E_R \approx 42$ meV, and $\alpha_R \approx 1.09$ eV Å in the valence band and $k_R \approx 0.004$ Å^{-1}, $E_R \approx 4$ meV, and $\alpha_R \approx 0.32$ eV Å in the conduction band, which are comparable to, if not larger than, typical values estimated at the surfaces of heavy metals such as Bi or Au. The FERSC behavior emerges when the ferroelectric polarization is reversed, leading to a complete switching of the spin texture, as it is clear by comparing Figs. 1(c) and 1(d). The switching can be understood as arising from a change of sign of the Rashba parameter α_R, which appears to depend linearly on the polar displacements (in analogy with the GeTe case [19]). Therefore, hyperferroelectrics can be considered as new multifunctional materials, where the control of the electric degrees of freedom has a direct consequence on the spin properties.

We now consider KMgBi. The band structure is similar to that shown in Fig. 1(a) for NaZnSb [26], with Rashba-like spin-split bands around the Γ point. The valence bands present a dominant Bi orbital character, while a mixture of Bi and Mg character is present in the conduction states. As for the case of NaZnSb, KMgBi belongs to the family of FERSCs, since the Rashba spin texture can be switched by switching the ferroelectric polarization. A crucial difference between the two compounds emerges when inspecting the orbital character around the band gap at the Γ point. Comparing Figs. 2(a) with 2(b), we note that the presence of SOC leads to an inverted gap where anionic (Bi) and cationic (Mg) characters are exchanged, while leaving an indirect band gap of about 0.1 eV. To assess the topological nature of KMgBi, we calculated the topological indexes following the adiabatic pumping of the Wannier charge centers [35,36], finding that KMgBi is a strong 3D topological insulator with (1;000) indices [26].

The first consequence of a nontrivial gap is the appearance of metallic massless surface states when the system is terminated by vacuum (semi-infinite slab with Mg-Bi termination) as shown in Fig. 2(c), where the Dirac point appears to be buried in the continuum of bulk states. Remarkably, the properties of the surface states appear to depend strongly on the nature of the termination and on the direction of the ferroelectric polarization. In Figs. 2(d) and 2(e), we show the calculated band structure for two opposite directions of ferroelectric polarization in the slab geometry, which allows us to consider the surface states of the inequivalent terminations in a single calculation. In this geometry, the bottom termination always comprises K ions, while the top one consists of Mg/Bi ions. Here we note that the slab calculations in Fig. 2 have been performed within the tight-binding framework to verify the bulk-edge correspondence, while neglecting possible self-consistent charge rearrangements at the surfaces due to the presence of polar terminations (K^+ and $[MgBi]^-$) [26]. Surface states arising from different terminations can then be identified by calculating the ionic character of the bands coming from superficial K or Mg/Bi ions. It is evident that the Dirac cones are buried in the bulk bands when the crystal terminates with K ions, even though a reversal of the ferroelectric polarization causes a significant modulation of the Dirac point position. On the other hand, at the MgBi termination the Dirac cone can be moved from the bulk valence continuum into the gap, close to the conduction bands. Even though the inequivalence of the surface states has been known as a characteristic feature of noncentrosymmetric TIs, we want to emphasize the strong tunability of the Dirac cones arising from the unique interplay with ferroelectricity. An in-gap energy cut reveals different Fermi surfaces and spin textures depending on the polarized state of the bulk system. For instance, at positive P the charge carriers from surface states would both show an n-type character, being above the corresponding Dirac cones, and opposite spin chiralities shown in Fig. 2(f).

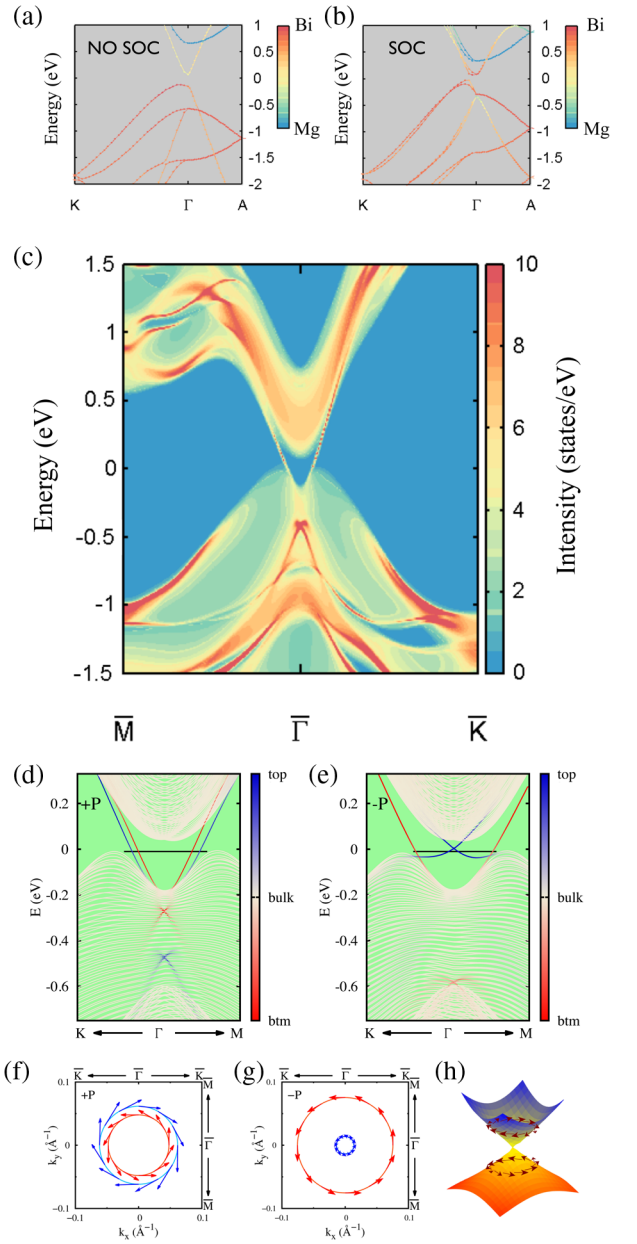

FIG. 2. Closeup at the Γ point around the Fermi level without (a) and with (b) SOC for KMgBi. (c) Surface spectral function for the (0001) hexagonal surface Brilouin zone where topological nontrivial surface states are visible inside the bulk band gap [26]. (d), (e) Surface states of KMgBi calculated in slab geometry for opposite direction of ferroelectric polarization. Characters of top (MgBi-terminated) and bottom (K-terminated) surface states are highlighted by the color scale, revealing that the Dirac cones of K-terminated surfaces are always buried in the continuum of bulk states. (f),(g) display spin textures of the surface states at the energy cut shown in panels (d),(e), while (h) shows that the chirality of spin polarization is reversed when crossing the Dirac cone.

However, when the polarization is reversed, the charge carriers at the top termination are holes, sharing the same spin chirality of bottom spin-polarized states [see Fig. 2(g)]. Side-by-side domain walls between different ferroelectric domains could behave then as intrinsic topological p-n

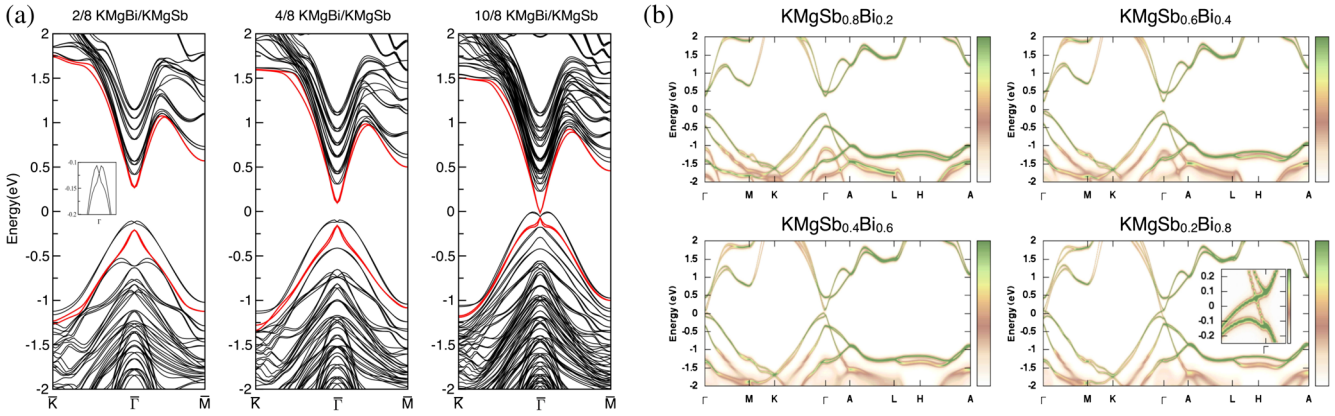

FIG. 3. (a) Band structures for 2/8, 4/8, and 10/8 KMgBi/KMgSb superlattice configurations along the high-symmetry directions $\bar{K}$-$\bar{\Gamma}$-$\bar{M}$. Red lines emphasise topologically nontrivial interfacial states emerging from the continuum of bulk bands (black lines), while the inset is a zoom of the valence Rashba bands. (b) Spectral functions for dilute $KMgSb_{1-x}Bi_x$ alloys at $x = 0.2$, 0.4, 0.6, and 0.8, respectively [26]. In the last panel, the inset reports a zoom around the Fermi level highlighting the Weyl semimetal phase. In this energy region, the three-dimensional nature of the Weyl fermions' dispersion ensures protection against the renormalization effects of disorder [37]. The finite bandwidth is only due to a finite $\delta = 10$ meV in the Green's function calculation [26].

junctions, with interesting implications for novel spintronic devices, as for example Veselago lens for electron current focusing or electron beam supercollimation [8,10]. Because of time-reversal symmetry, surface states above and below a Dirac point would always show opposite spin chirality, as shown in Fig. 2(h).

We recall here that an important property of HHs is their ability to sustain a ferroelectric polarization down to single atomic layers, even when interfaced with a normal insulator or confined in a slab geometry terminated by vacuum [24]. Therefore, HHs are suitable systems for studying the interplay between ferroelectric and spin properties in the low dimensional limit. We placed topologically nontrivial KMgBi in superlattice configurations with thick slabs of topologically trivial KMgSb (hereafter we adopt the same n/m $ABC/A'B'C'$ notation used in Ref. [24]). In Fig. 3(a) we report the band structures for 2/8, 4/8, 10/8 KMgBi/KMgSb superlattices, corresponding to about 0.8, 1.6, and 4.0 nm of topological thin films, respectively, embedded in a polar trivial host. Standard ferroelectrics (i.e., not hyperferroelectrics) will not polarize in this ultrathin geometry, while we checked that KMgBi remains polar even for the thinner 2/8 superlattice configuration (with KMgSb both in the polar and centrosymmetric phases). A polar structure is confirmed by the Rashba-split bands [see inset in Fig. 3(a)], whose chiralities are electrically controllable by acting on the ferroelectric polarization. Moreover, the topological nature of KMgBi thin films leads to the appearance of topologically protected interfacial states [red lines in Fig. 3(a)], becoming gapless when the interaction between the two KMgBi/KMgSb interfaces vanishes (as for the 10/8 configuration). Unlike for the slab geometry, where the surfaces are terminated by vacuum, superlattices' interfacial electronic structures do not show, by construction, a dependence on the polarization direction, and Dirac cone localized at the top and bottom interfaces are degenerate in energy.

A further interesting characteristic of topological (hyper) ferroelectrics is their capacity to undergo a finite intermediate Weyl semimetal phase during the topological transition from three-dimensional topological to normal insulators as a consequence of the broken inversion symmetry [12–14]. In fact, as shown in Fig. 3(b), tuning the relative Bi/Sb ratio in a dilute $KMgSb_{1-x}Bi_x$ alloy brings the system toward a topological transition marked by a gap closure [26]. In this semimetal phase of finite concentration extension ($0.65 < x < 0.90$) [26], bands linearly cross around the Fermi level [see inset in Fig. 3(b) for the case of $KMgSb_{0.2}Bi_{0.8}$], giving rise to a Weyl semimetal phase [11]. It is worth noting that such a phase is protected against the broadening effects of disorder, as a natural consequence of the three-dimensional nature of its electronic structure [37]. Furthermore, the distinct power law of the density of states within the Weyl phase [i.e., $D(\omega) \propto \omega^2$] leads to a change of exponents in the temperature dependence of thermodynamic quantities such as the specific heat ($C_V \sim T^3$) and compressibility ($\kappa \sim T^2$) [38], making this phase easily discernable by means of thermodynamics measurements. Moreover, we argue that the chirality of any Weyl fermion is electrically switchable by reversing the ferroelectric polarization.

Conclusions.—In summary, we have considered the role of relativistic SOC in the family of recently predicted hexagonal hyperferroelectrics, unveiling an extremely rich physics that is strongly intertwined with ferroelectric functionalities. Focusing our attention on two prototypical systems, namely, NaZnSb and KMgBi, we found that electrically tunable bulk Rashba spin splittings dominate the low-energy features of the band structure, putting forward HHs as new FERSC whose cross-coupled functionalities should persist in the limit of quasi-2D thin films. Increasing the strength of SOC, e.g., by replacing Sb with Bi, may lead to a strong 3D topological insulating phase, with the concomitant appearance of massless Dirac fermions at

inequivalent surfaces. The Dirac cones are found to be strongly modulated by the ferroelectric switching, opening interesting perspectives, e.g., for domain engineering and control of topological *p-n* junctions [10]. We further investigated the properties of heterostructures where a few layers of HH KMgBi are interfaced with a normal (and topologically trivial) ferroelectric; while the hyperferroelectric nature of KMgBi is confirmed by persistent polar distortions even in the limit of a few atomic layers, we found that changing the thickness of the HH layer allows for a tuning of the bulk band gap and for the appearance of topological interface states. Finally, we showed that a Weyl semimetal phase can be achieved by alloying KMgBi in a diluite solution with a topologically trivial hyperferroelectric.

We acknowledge CINECA for providing us computational resources and Henry cluster from North Carolina State University. D. D. S. and A. S. acknowledge the CARIPLO Foundation through the MAGISTER Project No. Rif. 2013-0726. D. V. acknowledges ONR Grant No. N00014-12-1-1035. The authors acknowledge A. Narayan for useful correspondence. D. D. S. acknowledges financial support from the German Research Foundation (DFG-SFB Project No. 1170).

Note added.—During the completion of the paper, we became aware of a theoretical study of Rashba effects in the class of hexagonal ferroelectrics [39]. On the other hand, in the present work we focus on the interplay between hyperferroelectricity and relativistic effects induced by SOC, including Rashba effect, 3D topological insulating, and Weyl semimetal phases.

*domenico.disante@physik.uni-wuerzburg.de

[1] M. Z. Hasan and C. L. Kane, Rev. Mod. Phys. **82**, 3045 (2010).
[2] X. L. Qi and S. C. Zhang, Rev. Mod. Phys. **83**, 1057 (2011).
[3] M. I. Dyakonov and V. I. Perel, Sov. Phys. JETP Lett. **13**, 467 (1971).
[4] Y. A. Bychkov and E. I. Rasha, Sov. Phys. JETP Lett. **39**, 78 (1984).
[5] T. H. Hsieh, H. Lin, J. Liu, W. Duan, A. Bansil, and L. Fu, Nat. Commun. **3**, 982 (2012).
[6] E. Plekhanov, P. Barone, D. Di Sante, and S. Picozzi, Phys. Rev. B **90**, 161108(R) (2014).
[7] O. V. Yazyev, J. E. Moore, and S. G. Louie, Phys. Rev. Lett. **105**, 266806 (2010).
[8] J. Wang, X. Chen, B.-F. Zhu, and S.-C. Zhang, Phys. Rev. B **85**, 235131 (2012).
[9] M. S. Bahramy, B.-J. Yang, R. Arita, and N. Nagaosa, Nat. Commun. **3**, 679 (2012).
[10] S. Liu, Y. Kim, L. Z. Tan, and A. M. Rappe, Nano Lett. **16**, 1663 (2016), and references [35–38] cited therein.
[11] X. Wan, A. M. Turner, A. Vishwanath, and S. Y. Savrasov, Phys. Rev. B **83**, 205101 (2011).
[12] J. Liu and D. Vanderbilt, Phys. Rev. B **90**, 155316 (2014).
[13] S. Murakami and S.-i. Kuga, Phys. Rev. B **78**, 165313 (2008).
[14] S. Murakami, New J. Phys. **9**, 356 (2007).
[15] M. S. Bahramy, R. Arita, and N. Nagaosa, Phys. Rev. B **84**, 041202(R) (2011).
[16] K. Ishizaka *et al.*, Nat. Mater. **10**, 521 (2011).
[17] Y. L. Chen, M. Kanou, Z. K. Liu, H. J. Zhang, J. A. Sobota, D. Leuenberger, S. K. Mo, B. Zhou, S.-L. Yang, P. S. Kirchmann *et al.*, Nat. Phys. **9**, 704 (2013).
[18] S. V. Eremeev, I. A. Nechaev, Y. M. Koroteev, P. M. Echenique, and E. V. Chulkov, Phys. Rev. Lett. **108**, 246802 (2012).
[19] D. Di Sante, P. Barone, R. Bertacco, and S. Picozzi, Adv. Mater. **25**, 509 (2013).
[20] S. Picozzi, Front. Phys. **2**, 10 (2014).
[21] M. Liebmann, C. Rinaldi, D. Di Sante, J. Kellner, C. Pauly, R. N. Wang, J. E. Boschker, A. Giussani, S. Bertoli, M. Cantoni *et al.*, Adv. Mater. **28**, 560 (2016).
[22] W. Zhong, R. D. King-Smith, and D. Vanderbilt, Phys. Rev. Lett. **72**, 3618 (1994).
[23] J. Junquera and P. Ghosez, Nature (London) **422**, 506 (2003).
[24] K. F. Garrity, K. M. Rabe, and D. Vanderbilt, Phys. Rev. Lett. **112**, 127601 (2014).
[25] J. W. Bennett, K. F. Garrity, K. M. Rabe, and D. Vanderbilt, Phys. Rev. Lett. **109**, 167602 (2012).
[26] See Supplemental Material at http://link.aps.org/supplemental/10.1103/PhysRevLett.117.076401 for computational methods, additional details on structural and electronic properties, and a list of compounds experimentally synthesized in the LiGaGe structure. Such systems potentially show hyperferroelectric properties. Interestingly, in many of them, heavy atoms like Bi, Sb, and Pb suggest the possibility of a nontrivial interplay with spin-orbit coupling. Furthermore, $LiNbO_3$ and $LiTaO_3$, recently predicted to be hyperferroelectrics (together with $LiVO_3$ and $LiOsO_3$), are well-known ferroelectric materials. $LiOsO_3$ is also widely studied as a "ferroelectric metal" [27,28]. The computational methods section includes also Refs. [29–34].
[27] P. Li, X. Ren, G.-C. Guo, and L. He, arXiv:1510.06835.
[28] Y. Shi, Y. Guo, X. Wang, A. J. Princep, D. Khalyavin, P. Manuel, Y. Michiue, A. Sato, K. Tsuda, S. Yu *et al.*, Nat. Mater. **12**, 1024 (2013).
[29] G. Kresse and J. Furthmüller, Phys. Rev. B **54**, 11169 (1996).
[30] J. Heyd, G. E. Scuseria, and M. Ernzerhof, J. Chem. Phys. **121**, 1187 (2004).
[31] A. A. Mostofi, J. R. Yates, Y.-S. Lee, I. Souza, D. Vanderbilt, and N. Marzari, Comput. Phys. Commun. **178**, 685 (2008).
[32] J. Henk and W. Schattke, Comput. Phys. Commun. **77**, 69 (1993).
[33] L. Fu and C. L. Kane, Phys. Rev. B **74**, 195312 (2006).
[34] L. Fu and C. L. Kane, Phys. Rev. B **76**, 045302 (2007).
[35] A. A. Soluyanov and D. Vanderbilt, Phys. Rev. B **83**, 235401 (2011).
[36] R. Yu, X. L. Qi, A. Bernevig, Z. Fang, and X. Dai, Phys. Rev. B **84**, 075119 (2011).
[37] D. Di Sante, P. Barone, E. Plekhanov, S. Ciuchi, and S. Picozzi, Sci. Rep. **5**, 11285 (2015).
[38] B.-J. Yang, M. S. Bahramy, R. Arita, H. Isobe, E.-G. Moon, and N. Nagaosa, Phys. Rev. Lett. **110**, 086402 (2013).
[39] A. Narayan, Phys. Rev. B **92**, 220101 (2015).